Progress In Electromagnetics Research M, Vol. 52, 45–56, 2016

Analysis of Microwave Scattering from a Realistic Human Head Model for Brain Stroke Detection Using Electromagnetic Impedance Tomography

Awais Munawar*, Zartasha Mustansar, and Adnan Maqsood

Abstract—Brain stroke incidences have arisen at an alarming rate over the past few decades. These strokes are not only life threatening, but also bring with them a very poor prognosis. There is a need to investigate the onset of stroke symptoms in a matter of few hours by the doctor. To address this, Electromagnetic Impedance Tomography (EMIT) employing microwave imaging technique is an emerging, cost-effective and portable brain stroke diagnostic modality. It has the potential for rapid stroke detection, classification and continuous brain monitoring. EMIT can supplement current brain imaging and diagnostic tools (CT, MRI or PET) due to its safe, non-ionizing and non-invasive features. It relies on the significant contrast between dielectric properties of the normal and abnormal brain tissues. In this paper, a comparison of microwave signals scattering from an anatomically realistic human head model in the presence and absence of brain stroke is presented. The head model also incorporates the heterogenic and frequency-dispersive behavior of brain tissues for the simulation setup. To study the interaction between microwave signals and the multilayer structure of head, a forward model has been formulated and evaluated using Finite Element Method (FEM). Specific Absorption Rate (SAR) analysis is also performed to comply with safety limits of the transmitted signals for minimum ionizing effects to brain tissues, while ensuring maximum signal penetration into the head.

1. INTRODUCTION

Brain stroke and Traumatic Brain Injuries (TBIs) are the third major cause of death in the world after heart and cancer diseases. They cause an interruption in the blood supply to the brain that result in the denial of oxygen and nutrients to the brain tissues. This phenomenon severely affects the main functions of the brain and may eventually result into death. Two major types of brain stroke are; hemorrhagic stroke and ischemic stroke [1]. The hemorrhagic stroke is caused by the rupture of blood vessels, whereas ischemic stroke is caused by the blockage of blood arteries [2, 3]. Some common symptoms exhibited by the both types of stroke and TBIs are; dizziness, slurred speech, difficult swallowing and sudden numbness of the body parts. An entirely different course of treatment is required for the cure of each type of disease. This establishes the urgency to reliably detect and classify the type of stroke by the doctor within a few hours from the onset of stroke symptoms [4].

The present brain stroke diagnostic techniques include both the imaging and non-imaging modalities. Methods like Computed Tomography (CT), Magnetic Resonance Imaging (MRI) and Positron Emission Tomography (PET) are known as imaging modalities, whereas Electro-encephalography (EEG), Magneto-encephalography (MEG), Electrical Impedance Tomography (EIT) and Magnetic Induction Tomography (MIT) are categorized as non-imaging modalities. More recently,

Received 13 August 2016, Accepted 2 October 2016, Scheduled 14 November 2016

* Corresponding author: Awais Munawar Qureshi (awaismunawar.phd06@rcms.nust.edu.pk).
The authors are with the Research Center for Modeling and Simulation (RCMS), National University of Sciences and Technology (NUST), H-12 Islamabad, Pakistan.

Electromagnetic Impedance Tomography (EMIT) employing microwave imaging technique has emerged as an alternate brain imaging modality. It relies on the significant contrast between dielectric properties of the normal and stroke-affected brain tissues. We performed a detailed comparison analysis using literature available to-date on the existing imaging modalities, and found out that EMIT is a cost-effective, portable and fast brain imaging technique. The exposure of low frequency (0.5–4.5 GHz) and low power ($\geq$ 0 dBm) microwave signals makes EMIT a safe, non-ionizing and non-invasive imaging option, suitable for continuous brain monitoring. In the emergency situations or at rural areas, EMIT can also supplement current brain imaging and diagnostic tools (CT, MRI or PET). Therefore, EMIT has been explored and proposed in this study for rapid brain stroke detection, differentiation and progression monitoring.

2. BACKGROUND

The first study in the field of microwave brain imaging was conducted by Lin and Clarke [5] in 1982, who experimentally detected the presence of cerebral edema in a rudimentary head phantom using a 2.4 GHz microwave signal. It was until year 2000 that this concept was further furnished by Haddad et al. [6] who detected hematoma in human brain using ultra-wideband signals. Their work was extended by Paulson et al. [7] in 2005 but that was of preliminary nature. However, it was the first time in 2007 that Semenov and Corfield [8] assessed the feasibility and performance potential of Microwave Tomography (MWT) for brain stroke detection. The analysis were based on computer simulations utilizing a simplified 2-D head model with an ischemic stroke and the microwave signal of 0.5–2.0 GHz frequency with 20 dBm transmitted power.

In 2010, Ireland and Bialkowski [9] conducted a feasibility study on brain stroke detection based on microwave signals propagation into an anatomically realistic human head phantom with emulated stroke [10]. Because, the development of image reconstruction algorithm requires Electric Field (E-field) information both inside brain and at receiver locations, the authors therefore calculated the E-field values using Finite-Difference Time-Domain (FDTD) numerical method in their simulations. In 2010, Zakaria et al. [11] demonstrated the capability of Finite Element Method (FEM) numerical solver and Contrast Source Inversion (CSI) image reconstruction method to detect the hemorrhagic stroke inside a simplified 2-D brain model. Based on the microwave signal propagation studies on brain stroke, later in 2011 Ireland and Bialkowski proposed an image reconstruction algorithm as an extension to their previous work [12]. This ultimately contributed another step towards the microwave head imaging. The inversion algorithm was based on common background reflections cancellation, the confocal delay-and-sum approach and the Fermat's principle. For further studies on these principles, reader is referred to [13–16]. The back-scattered signals were estimated using a Gaussian pulse transmitted signal (0.5–2.0 GHz at 20 dB SNR), the Zubal head phantom with hemorrhagic stroke [10] and the 2-D FDTD forward solver.

In 2012, Scapaticci et al. [17] provided design guidelines to select the most convenient working frequency (0.6–1.5 GHz) and the optimum matching medium dielectric properties ($\epsilon_{\mathrm{mm}} = 40$, $\sigma_{\mathrm{mm}} = 0.01$ S/m) for the microwave imaging setup. The performance of imaging strategy, based on modified Linear Sampling Method (LSM) for brain stroke evolution monitoring, was also evaluated. The scattered field data was collected using the Zubal head phantom with ischemic stroke [10] and the Method of Moment (MoM) forward solver. In 2013, an analytical model was formulated by Jalilvand et al. [18] for brain stroke detection using ultra-wide band (UWB) radar approach. In order to explain the UWB signals (up to 10 GHz) propagation inside the stroke affected multi-layer head model, the authors investigated both the reflection and transmission scenarios. In the radar approach, the backscattered signals are utilized to create images that indicate the location of significant scatterers only (stroke, tumor). Once compared with MWT approach, in MWT the transmitted and backscattered fields are utilized to obtain shape of the object as well as the spatial distribution of dielectric properties by solving inverse scattering problem.

Major progress in the field of microwave imaging of head for brain stroke analysis was made during the year 2013. Fhager et al. [19] proposed a microwave-helmet based imaging setup for the detection of brain strokes. The helmet comprised of 10–12 triangular patch antennas (0.1–3.0 GHz) and flexible plastic bags filled with matching liquid for head adjustment. A statistical classifier algorithm

was also developed to differentiate two types of stroke. By contrast, a similar idea but utilizing an adjustable platform mounted with an array of tapered slot antennas (1–4 GHz) was proposed by Mohammed et al. [20] and Abbosh [21] for microwave head imaging. The later approach also applied a preprocessing technique to remove background reflections' noise from the received signals [22] and the image reconstruction algorithm was based on confocal delay-and-sum approach and the Fermat's principle. Using similar system, Mohammed, et al. [23] and Mobashsher et al. [24] investigated the possibility to differentiate two types of brain stroke. The methodology was respectively based on the comparison of reflection coefficients (S_{11}) or reflection phases of any pair of antennas located symmetrically around the head. In the same year, Priyadarshini and Rajkumar [25] performed an EM waves scattering analysis for brain stroke diagnostics using FEM-CSI methodology but on a simplified ellipsoid head model.

In 2014, a portable microwave system was presented by Mobashsher and Abbosh [26, 27] to detect the intracranial hemorrhage and TBIs. The wideband system was based on a virtual array mono-static radar approach utilizing a unidirectional antenna (1.1–3.4 GHz). In 2016, Mobashsher et al. [28] also performed a design and experimental evaluation of the microwave head imaging system for intracranial hemorrhagic detection using a modified delay-and-sum back-projection inversion algorithm. Both these studies followed the radar approach to indicate the location of hemorrhagic stroke using delay-and-sum back-projection inversion algorithm. A tomographic image of the brain, highlighting each layer of tissue, was not provided to have a complete picture of stroke affected brain.

In this paper, we have presented a comparison analysis of microwave signals scattering from an anatomically realistic human head model in the presence and absence of different types of stroke using Finite Element Method (FEM) method. FEM is selected due to its ability to model complex and arbitrary shaped geometries. Specific Absorption Rate (SAR) analysis is also presented to cater safety limits of microwave signals exposure to human brain. At the end, a Contrast Source Inversion (CSI) based image reconstruction algorithm is proposed to obtain a detailed tomographic picture of the brain for stroke detection and differentiation.

The development of microwave head imaging system starts with the modeling of an anatomically realistic and structurally detailed human head model. These numerical head models are based on either MRI images or CT data sets. One of the most frequently utilized head phantom involved in numerical head modeling is proposed by Zubal et al. [10]. The Zubal head phantom is based on MRI images and freely accessible too [29]. The developers of the Zubal head phantom have also provided a list of segmentation IDs to indicate different layers of head tissues. In our present research, we have also utilized the Zubal head phantom MRI database to construct a detailed numerical head model.

The numerical head models should incorporate the heterogenic and frequency-dispersive behavior of brain tissues. The dielectric properties (ϵ; permittivity and σ; conductivity) to different types of head tissues are assigned using either the averaged values or the frequency-dispersive models. S. Gabriel and C. Gabriel modified the N-term Cole-Cole model [30] to adapt for assignment of dielectric properties to different types of body tissues. It is termed as 4-term Cole-Cole model and is valid across 10 Hz to 20 GHz frequency range [31–35]. Andreuccetti et al. [36] converted the 4-term Cole-Cole model into an online frequency dependent application/database repository. Later on, Ireland and Abbosh [37] and Mustafa et al. [38] optimized the N-term Debye model to 2-term/4-term Debye models, respectively. These models were computationally less intensive and explicit to calculate dielectric properties of seventeen different types of head tissues in the microwave frequency band. The 4-term Debye model provided more accurate results with lower computational overheads as compared to the 4-term Cole-Cole model across the microwave frequency range (0.1–3 GHz).

3. METHODOLOGY

Microwave imaging (MWI) has been widely utilized in many industrial and medical imaging applications. The object-of-interest (OI) is illuminated by a single or multiple microwave signal sources either at one frequency or multi-frequency. The scattered or reflected signals from the OI are measured at various receiver locations around the OI. Based on these measured field values, the dielectric properties of the OI are calculated and processed to construct the object images in the presence of known surrounding medium [39]. The EMIT microwave imaging technique makes use of significant contrast between

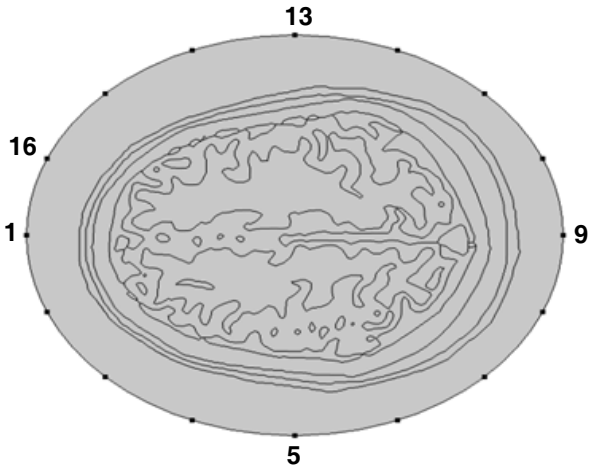

Figure 1. 2-D Layout of an EMIT-based head imaging system.

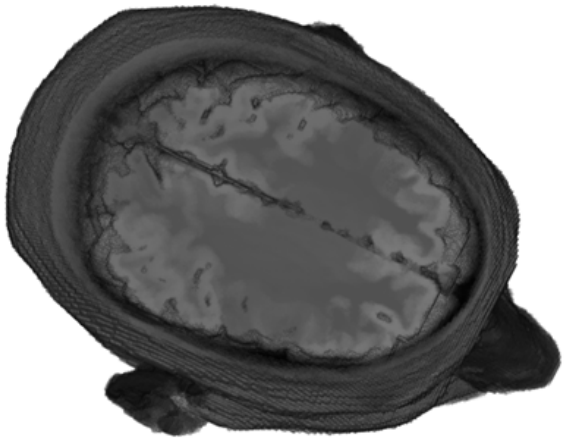

Figure 2. 3-D Cross-sectional view of the Zubal head phantom.

dielectric properties of body tissues to distinguish the normal and abnormal regions. Primarily, two approaches are being followed in active MWI [18]; the Confocal Radar Technique [40] and the Classical Inverse Scattering/MWT [41]. The basic layout of EMIT-based head imaging system comprises an array of transmitter-receiver antennas that operates in a sequential mode around the head. A 2-D layout of our proposed EMIT-based head imaging setup, comprising an array of 16 point current sources that surround an anatomically realistic human head model is shown in Figure 1. It is highlighted that microwave signals, transmitted at 0.5–4.5 GHz frequency with power level ≥ 0 dBm, offer a reasonable compromise between signal penetration into the head and the acceptable spatial resolution of the brain images [20].

3.1. Numerical Head Model

In our simulation studies, we have developed an anatomically realistic human head numerical model utilizing the Zubal head phantom MRI database [29]. The MRI images were imported into Simpleware ScanIP image processing suite. Different types of head tissues were segmented according to phantom developer's tissue ID list. A 3-D cross-sectional view of the Zubal head phantom plotted in ImageJ freeware software is shown in Figure 2. The Zubal head phantom volume comprises $256 \times 256 \times 128$ cubical elements with $1.1\,\text{mm} \times 1.1\,\text{mm} \times 1.4\,\text{mm}$ voxel size.

A 2-D image of the Zubal head phantom slice 36 was exported from Simpleware ScanIP as NASTRAN mesh format after requisite pre-processing steps. The geometry of slice 36 was generated from the exported mesh for use in electromagnetic simulation environment. We have selected slice 36 of the Zubal head phantom in our 2-D simulation studies because it not only incorporates the major six types of brain tissues but also simplifies the simulation problem. Moreover, it also provided us an opportunity to compare our simulation results with earlier studies mostly involving slice 36 of phantom. The frequency-dispersive dielectric properties to different types of head tissues were allocated using Andreuccetti et al. [36] online repository. Figure 3 shows the relative permittivity (ϵ_r) and conductivity (σ) assignment to the Zubal head phantom tissues (slice 36) at 1 GHz frequency with emulated hemorrhagic stroke.

3.2. Forward Problem Modeling

The forward problem modeling and analysis provides us the basic guidelines to develop an anatomically realistic human head model, the placement of microwave transceivers and the suitable frequency range of transmitted signal at allowable power levels. In this paper, we have restricted ourselves to 2-D forward model simulations for proof of our proposed methodology in a time efficient manner. Sixteen

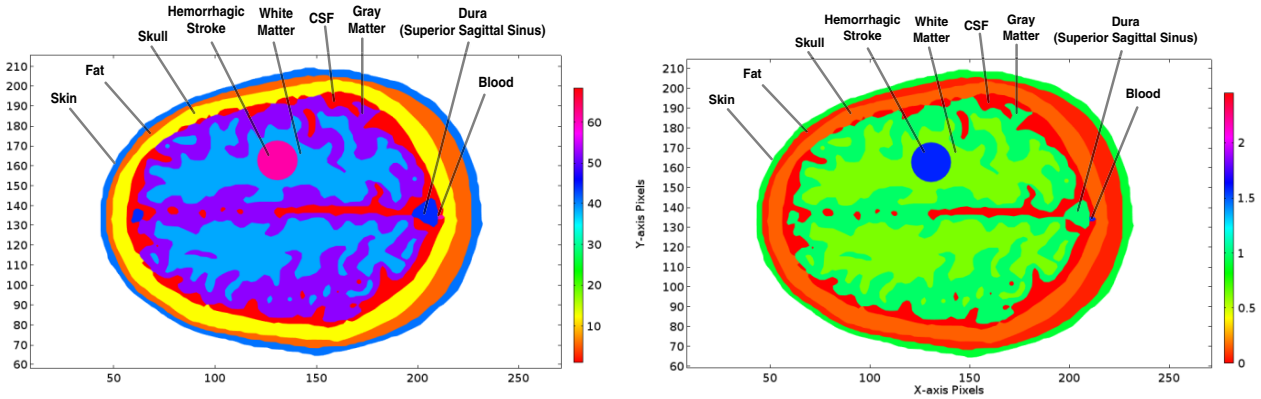

Figure 3. Relative permittivity and conductivity profile of the Zubal head phantom slice 36 at 1 GHz. (a) Relative permittivity. (b) Electrical conductivity.

point current sources are arranged in an elliptical array around the Zubal head phantom (slice 36) with equidistant separation in the simulation environment. Each point source is placed at 2–3 cm distance from the side of head phantom and operates at 1 mA current. They transmit a Transverse Magnetic (TM) polarized microwave signal at 1 GHz frequency in a sequential fashion. The computational domain around the head is truncated using Perfectly Matched Layer (PML) with Absorbing Boundary Condition (ABC). The continuity boundary conditions are applied between air and head phantom or different layers of the brain tissues using Equation (1), where E is the electric field intensity [V/m].

$$\hat{\mathbf{n}} \times (\vec{\mathbf{E}}_1 - \vec{\mathbf{E}}_2) = 0 \tag{1}$$

The evaluation of interaction between microwave signals and human head model requires the solution of above explained forward problem model. Several numerical methods are employed to calculate electric field values at numerous locations by solving Maxwell's equations. Finite-Difference Time-Domain (FDTD), Method of Moments (MoM), Boundary Element Method (BEM) and Finite Element Method (FEM) are among the few numerical techniques which are being adopted in microwave imaging forward solvers [42]. In this study, we have proposed to apply FEM, a numerical method to solve forward problem model in frequency domain. FEM solves the Helmholtz vector wave equation (Equation (2)), derived from Maxwell's equations in time-harmonic form, to find electric field values of transmitted and backscattered microwave signals. FEM is preferred over other numerical methods due to its flexibility to address irregular geometries, anisotropic dielectric materials and inhomogeneous background medium with least discretization errors. FEM is also more suitable for performing steady-state analysis of the problem once compared to FDTD or MoM numerical methods.

$$\boldsymbol{\nabla} \times \mu_r^{-1}(\boldsymbol{\nabla} \times \vec{\mathbf{E}}) - k_0^2 \left(\varepsilon_r - \frac{j\sigma}{\omega\varepsilon_0}\right) \vec{\mathbf{E}} = 0 \tag{2}$$

where μ_r is the relative permeability (H/m), ε_r the relative permittivity (F/m), ω the angular frequency (rad/s), σ the electric conductivity [S/m], and $k_0 = \omega\sqrt{\mu_0\epsilon_0}$ the free-space wave number (m^{-1}).

In our 2-D case study, the FE mesh comprised 25,568 triangular and 140 quadrilateral elements with 2,654 edges and 963 vertices. In order for solution to converge, the criterion of at least 05 elements per wavelength was considered. There were at least 180,713 number degrees of freedom in the FE mesh and the solution convergence time was approximately 20 secs. The simulation was run on Intel Core i7 dual core processor (2.4 GHz) with 16 GB RAM workstation. Figure 4 shows the spatial distribution of normalized electric field (E-Norm) inside the Zubal head phantom (slice 36) in the absence and presence of hemorrhagic stroke with point source located at position 13. In the figure, the color bar represents E-Norm value (V/m) with red color indicating the location of higher E-Norm values and the blue color highlighting the regions of lower values.

A hemorrhagic stroke of circle shape with 20 mm diameter was emulated in the white matter region with blood dielectric properties, whereas for the normal head phantom, the stroke circle was assigned

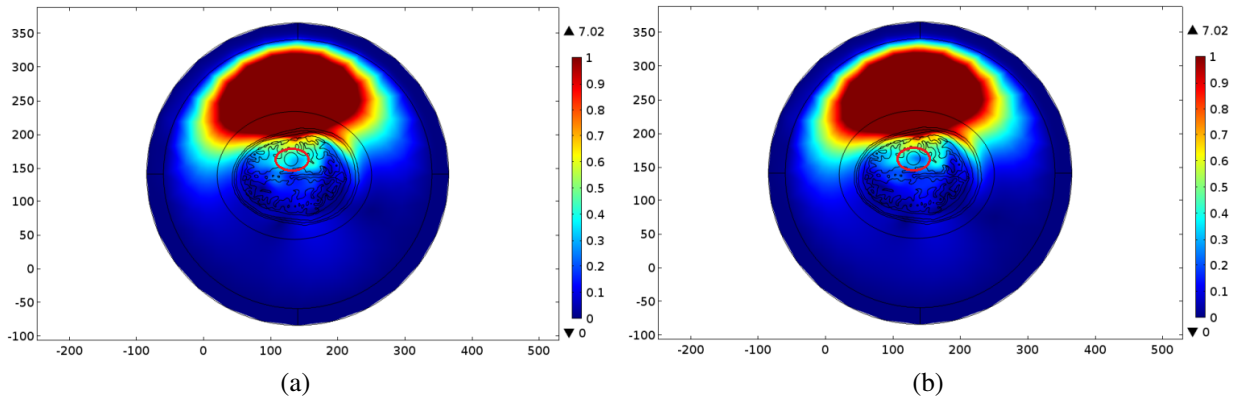

Figure 4. Spatial distribution of normalized E-field inside the Zubal head phantom (slice 36) at 1 GHz. (a) Normal head phantom. (b) Hemorrhagic stroke affected head phantom.

white matter dielectric properties. In normal case (Figure 4(a)) the penetration of E-field is more progressive and uniform as it encounters tissue layers of different dielectric properties. By contrast, in hemorrhagic stroke case (Figure 4(b)) the penetration is less due to in-homogenous dielectric properties of stroke tissues emulated inside white matter region. It has been observed that there is a significant contrast in the pattern of electric field distribution for two different cases at stroke location (encircled red). E-Norm values were calculated for both cases at different locations of stroke area. The maximum E-Norm absolute difference at same point inside stroke region is measured as 0.076 V/m, with E-Norm value of 0.299 V/m for normal tissues and 0.223 V/m for hemorrhagic affected tissues. In results and discussion section, Figure 6(a) shows the E-Norm absolute difference distribution inside the Zubal head phantom (slice 36) for hemorrhagic affected tissues with respect to normal brain tissues.

3.3. Inverse Problem Solution

Microwave imaging inverse problem is a mathematically nonlinear and ill-posed problem comprising a large number of unknowns. The brain images are reconstructed using spatial distribution of dielectric properties of the brain tissues. The image reconstruction algorithm utilizes transmitted and backscattered electromagnetic fields information obtained from forward problem solution. An appropriate image reconstruction method is selected based upon application in hand. The most frequently utilized non-linear inversion methods include; Contrast Source Inversion (CSI), Gauss-Newton Inversion (GNI), Confocal Delay-and-Sum Algorithm and Born Iterative Method (BIM) [11, 12, 20, 22, 43, 44].

A literature based analysis was performed to compare the accuracy and computational efficiency of different inversion methods suitable for microwave head imaging setup. It was found out that Contrast Source Inversion (CSI) or Multiplicative Regularized CSI (MR-CSI) is preferred over other methods due to its independence on forward solution recalls during multiple iterations [11, 45]. Therefore, CSI is proposed to solve the inverse scattering problem of calculating brain tissues' dielectric profiles and reconstructing brain images for stroke detection. In our future studies, we will develop an efficient image reconstruction algorithm based upon FEM-CSI methodology in MATLAB® environment. Different types of stroke will be investigated, localized and classified using developed inversion algorithm. In order to make the applications time-efficient, parallel processing techniques will also be considered in solving forward and inverse problems for multi-frequency and multi-source scenarios using core/thread allocation schemes.

3.4. Specific Absorption Rate (SAR) Analysis

SAR analysis helps in determining the amount of radiations absorbed by human body tissues and the temperature increase incurred, once exposed to electromagnetic signals. Several studies have been conducted to calculate SAR values for human head tissues using mobile phones. Some of these involved

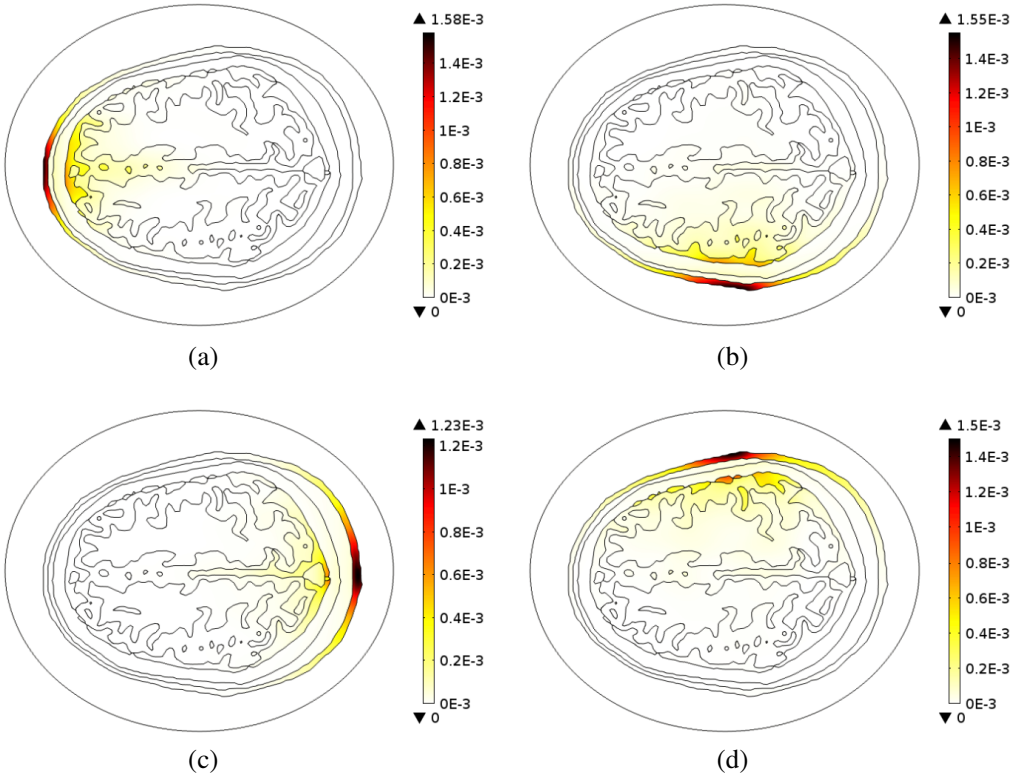

Figure 5. SAR distribution inside the Zubal head phantom (slice 36) at 1 GHz frequency. (a) Point source located at position 1. (b) Point source located at position 5. (c) Point source located at position 9. (d) Point source located at position 13.

computer simulations utilizing numerical head models [46–49], whereas some were based on theoretical analysis [50]. SAR is defined as the amount of power dissipated per unit mass and measured in watts per kilogram [W/kg]. SAR values are calculated using Equation (3), where σ is tissue electric conductivity [S/m], ρ is tissue density [kg/m^3] and E is induced electric field intensity norm value [V/m].

$$SAR = \frac{\sigma E^2}{2\rho} \tag{3}$$

We have also performed SAR analysis of our proposed EMIT based head imaging setup. The simulation setup utilized point current sources (1 mA, 1 GHz frequency) positioned at 2–3 cm distance from the side of numerical head model. Figure 5 shows the SAR distribution for four different locations of point current sources (1, 5, 9 & 13). It has been observed that in all four cases, the maximum local SAR value (1.58e^{-3} W/kg) is calculated for point current source located in front of head phantom at location 1. This value is far below the safety limits of average SAR (2 W/kg over 10 g of tissue) as per IEEE EM safety standard (C95.1-2005) [51] and ICNIRP non-ionizing radiation protection guidelines [52]. In the figure, the thermal color bar represents local SAR value (W/Kg) with reddish brown color indicating the location of higher SAR values and the white color highlighting the regions of lower values. Moreover, the maximum SAR value is observed at skin layer which dissipates gradually as the microwave signals move into the head phantom.

During our literature review, we have also determined that a microwave signal (0.5–4.5 GHz) with 0–20 dBm power, transmitted at 2–4 cm distance from the side of head phantom, would be sufficient for reconstructing reliable brain images with minimum ionizing effects. Mobashsher, et al. [28] performed SAR analysis on the Zubal head phantom using Dipole antenna with transmission power of 0 dBm at 1.1–3.2 GHz frequency. The peak SAR value 16e^{-3} W/kg calculated at 1.8 GHz was also lower than 2 W/kg. The SAR value calculated at 1.1 GHz frequency for Dipole antenna located at position 1 was

$4e^{-3}$ W/kg. In our simulations, point current source (1 mA, 1 GHz frequency) located at position 1 produces $1.58e^{-3}$ W/kg SAR value which approximately validates the previous results.

4. RESULTS AND DISCUSSION

The feasibility of microwave imaging for brain stroke detection, localization and differentiation can be well understood from the analysis of different simulation studies. Figure 6 shows the normalized electric field absolute difference distribution inside the Zubal head phantom (slice 36) for two different types of emulated stroke with respect to normal brain model. The point source is located at position 13 and operating at 1 GHz frequency with 1 mA current. In the figure, the color bar represents absolute difference of E-Norm (V/m) with red color indicating the location of greater absolute difference and the blue color highlighting the regions of smaller absolute differences. It has been observed that maximum E-Norm absolute difference exists at approximate location of the stroke in both cases. This significant contrast can be effectively utilized in the development of image reconstruction algorithm for the brain, based upon the calculation of tissues' dielectric profiles from scattered electric field information.

We have compared our simulation results on microwave scattering from normal/stroke affected human head model with earlier research studies as well [37, 38]. It is pertinent to highlight that our facts and figures matched them quite well. The previous studies were performed using FDTD numerical method to solve the forward problem model in time-domain. In our research, we have utilized FEM numerical technique to solve the forward problem model in frequency-domain. This approach not only addresses the complex structure of brain in an appropriate way but also performs the steady-state analysis of microwave scattering phenomenon in a time-efficient manner. Multi-frequency swept technique is also implemented to analyze the microwave scattering phenomenon from stroke affected human brain model at different frequencies.

In this simulation study, each point current source operates in a sequential mode around the head phantom and scattered E-Norm field is measured at rest of locations. Simulations have been performed for both normal and stroke affected brain models (Hemorrhagic and Ischemic). Figure 7 shows the scaled absolute difference plot for scattered E-Norm values for both types of stroke with respect to normal head tissues. It has been observed that the values of absolute difference E-Norm were greater in case of hemorrhagic stroke as compared to ischemic stroke. It is due the fact that dielectric properties of hemorrhagic stroke contrast considerably with respect to white matter. Whereas, the ischemic stroke dielectric properties are much closer to white matter and the stroke is emulated in white matter region too. Therefore, as the microwave signals travel in to brain they face more scattering phenomenon in case of hemorrhagic stroke as compared to ischemic stroke.

In case of hemorrhagic stroke, the change in scattered E-Norm values is more obvious once the point source is placed at location 3/4/7 or 13/14 and E-Norm is measured at location 13/14 or 3/4/7 respectively. Whereas in case of Ischemic stroke, point source placed at 4, 13 and 14 produces significant

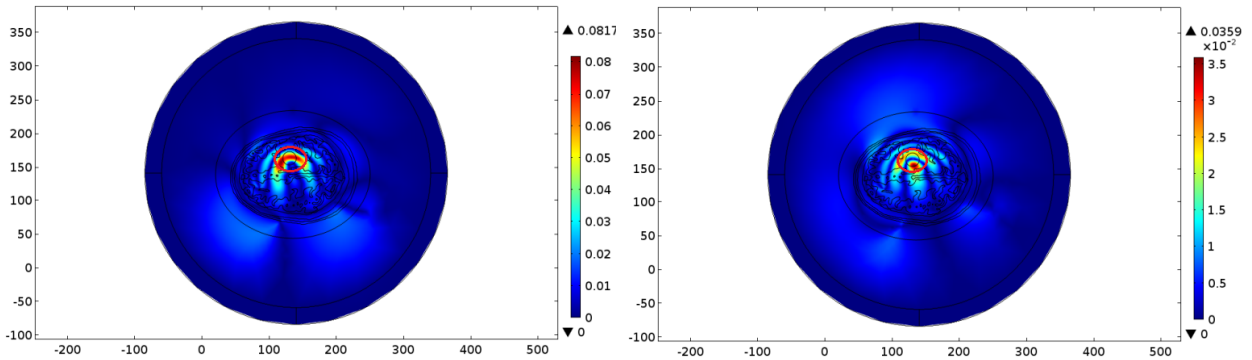

Figure 6. E-Norm absolute difference inside the Zubal head phantom with point source at position 13. (a) Hemorrhagic stroke emulated. (b) Ischemic stroke emulated.

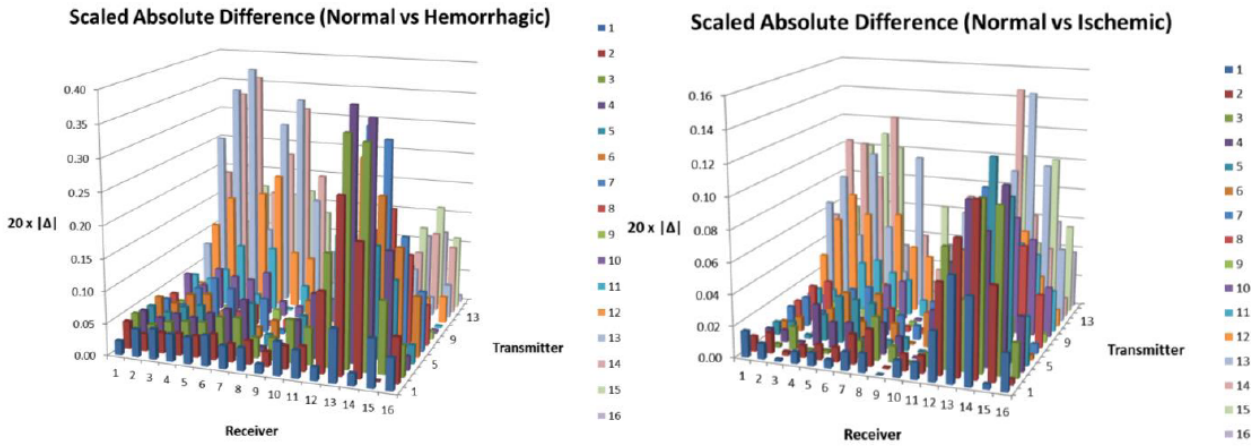

(a) (b)

Figure 7. Scaled absolute difference plot for scattered E-Norm at different locations for each transmitter. (a) Hemorrhagic stroke emulated. (b) Ischemic stroke emulated.

change in scattered E-Norm values at location 15, 14 and 5 respectively. High E-Norm absolute difference is observed at receiver locations which are either opposite to the transmitters in line of stroke (transmission changes) or adjacent to the transmitters (reflection changes). We have compared our microwave scattering 3-D plot of scaled absolute E-Norm difference for hemorrhagic stroke with earlier studies [9] and it has shown good consistency with their results as well.

5. CONCLUSION

In this paper, we have presented a 2-D simulation setup for brain stroke detection based upon Electromagnetic Impedance Tomography approach using microwave signals. The feasibility of the system has been evaluated by performing microwave scattering analysis from an anatomically realistic human head model. It has been observed that the scattered electric field values at different locations around the head can be efficiently utilized to determine the significant contrast in dielectric profile of brain tissues at stroke location. FEM-CSI methodology has been proposed for performing microwave scattering analysis from human head model and developing image reconstruction algorithm for accurate brain stroke detection, localization and differentiation. SAR analysis of proposed brain imaging technique was also performed to take into account the electromagnetic signals' safe exposure to human head.

In future, an efficient image reconstruction algorithm will be developed for head imaging, based upon scattered electric field information obtained from 2-D simulation setup. Multi-frequency swept technique will also be incorporated during microwave scattering analysis of human head model and the development of image reconstruction algorithm. This approach will allow us to construct better quality images of the brain for stroke analysis. A 3-D forward model setup will be formulated to study the microwave scattering phenomenon from a 3-D anatomically realistic human head model for brain stroke analysis. Parallel processing techniques will also be considered in forward and inverse problem models to develop time-efficient applications involving multi-frequency and multi-source scenarios. Efforts will also be made in suggesting optimum technical characteristics of the design setup for a prototype EMIT-based head imaging system for brain stroke localization and classification.

REFERENCES

1. Stroke (Cerebrovascular Accident), Hemorrhagic, Discharge Information, [Online]. Available: http://www.summitmedicalgroup.com/library/adult_care/ac-strokehemorrhagic_dc/.

2. Feigin, V. L., "Stroke epidemiology in the developing world," *The Lancet*, Vol. 365, 2160–2161, 2005.
3. The Internet Stroke Center, [Online]. Available: http://www.strokecenter.org/.
4. Khan, F., I. J. Baguley, and I. D. Cameron, "4: Rehabilitation after traumatic brain injury," *Med. J. Aust.*, Vol. 178, 290-5, Mar. 17, 2003.
5. Lin, J. C. and M. J. Clarke, "Microwave imaging of cerebral edema," *Proceedings of the IEEE*, Vol. 70, 523–524, 1982.
6. Haddad, W., J. Chang, T. Rosenbury, G. Dallum, P. Welsh, D. Scott, et al., "Microwave hematoma detector for the rapid assessment of head injuries," *Lawrence Livermore National Laboratory Technical Report UCRL-ID*, Vol. 137901, 2000.
7. Paulson, C. N., J. T. Chang, C. E. Romero, J. Watson, F. J. Pearce, and N. Levin, "Ultra-wideband radar methods and techniques of medical sensing and imaging," *Optics East 2005*, 60070L-60070L-12, 2005.
8. Semenov, S. Y. and D. R. Corfield, "Microwave tomography for brain imaging: Feasibility assessment for stroke detection," *International Journal of Antennas and Propagation*, Vol. 2008, 1–8, 2008.
9. Ireland, D. and M. Bialkowski, "Feasibility study on microwave stroke detection using a realistic phantom and the FDTD method," *Asia-Pacific Microwave Conference 2010*, 1–4, 2010.
10. Zubal, I. G., C. R. Harrell, E. O. Smith, Z. Rattner, G. Gindi, and P. B. Hoffer, "Computerized three-dimensional segmented human anatomy," *Medical physics*, Vol. 21, 299–302, 1994.
11. Zakaria, A., C. Gilmore, and J. LoVetri, "Finite-element contrast source inversion method for microwave imaging," *Inverse Problems*, Vol. 26, 115010, 2010.
12. Ireland, D. and M. E. Bialkowski, "Microwave head imaging for stroke detection," *Progress In Electromagnetics Research M*, Vol. 21, 163–175, 2011.
13. Bialkowski, M. and Y. Wang, "UWB cylindrical microwave imaging system employing virtual array antenna concept for background effect removal," *Microwave and Optical Technology Letters*, Vol. 53, 1100–1104, 2011.
14. Bialkowski, M. E., "Ultra wideband microwave system with novel image reconstruction strategies for breast cancer detection," *2010 European Microwave Conference (EuMC)*, 537–540, 2010.
15. Li, X. and S. C. Hagness, "A confocal microwave imaging algorithm for breast cancer detection," *IEEE Microwave and Wireless Components Letters*, Vol. 11, 130–132, 2001.
16. Bialkowski, M. E., Y. Wang, A. Abu Bakar, and W. C. Khor, "Novel image reconstruction algorithm for a UWB cylindrical microwave imaging system," *2010 IEEE MTT-S International Microwave Symposium Digest (MTT)*, 477–480, 2010.
17. Scapaticci, R., L. Di Donato, I. Catapano, and L. Crocco, "A feasibility study on microwave imaging for brain stroke monitoring," *Progress In Electromagnetics Research B*, Vol. 40, 305–324, 2012.
18. Jalilvand, M., X. Li, and T. Zwick, "A model approach to the analytical analysis of stroke detection using UWB radar," *2013 7th European Conference on Antennas and Propagation (EuCAP)*, 1555–1559, 2013.
19. Fhager, A., Y. Yu, T. McKelvey, and M. Persson, "Stroke diagnostics with a microwave helmet," *2013 7th European Conference on Antennas and Propagation (EuCAP)*, 845–846, 2013.
20. Mohammed, B. J., A. M. Abbosh, S. Mustafa, and D. Ireland, "Microwave system for head imaging," *IEEE Transactions on Instrumentation and Measurement*, Vol. 63, 117–123, 2014.
21. Abbosh, A., "Microwave systems for head imaging: Challenges and recent developments," *2013 IEEE MTT-S International Microwave Workshop Series on RF and Wireless Technologies for Biomedical and Healthcare Applications (IMWS-BIO)*, 2013.
22. Mustafa, S., B. Mohammed, and A. Abbosh, "Novel preprocessing techniques for accurate microwave imaging of human brain," *IEEE Antennas and Wireless Propagation Letters*, Vol. 12, 460–463, 2013.

23. Mohammed, B., A. Abbosh, and D. Ireland, "Stroke detection based on variations in reflection coefficients of wideband antennas," *2012 IEEE Antennas and Propagation Society International Symposium (APSURSI)*, 1–2, 2012.
24. Mobashsher, A. T., B. Mohammed, A. Abbosh, and S. Mustafa, "Detection and differentiation of brain strokes by comparing the reflection phases with wideband unidirectional antennas," *2013 International Conference on Electromagnetics in Advanced Applications (ICEAA)*, 1283–1285, 2013.
25. Priyadarshini, N. and E. Rajkumar, "Finite element modeling of scattered electromagnetic waves for stroke analysis," *2013 35th Annual International Conference of the IEEE Engineering in Medicine and Biology Society (EMBC)*, 2404–2407, 2013.
26. Mobashsher, A. T., A. M. Abbosh, and Y. Wang, "Microwave system to detect traumatic brain injuries using compact unidirectional antenna and wideband transceiver with verification on realistic head phantom," *IEEE Transactions on Microwave Theory and Techniques*, Vol. 62, 1826–1836, 2014.
27. Mobashsher, A. T. and A. Abbosh, "Microwave imaging system to provide portable-low-powered medical facility for the detection of intracranial hemorrhage," *2014 1st Australian Microwave Symposium (AMS)*, 23–24, 2014.
28. Mobashsher, A., K. Bialkowski, A. Abbosh, and S. Crozier, "Design and experimental evaluation of a non-invasive microwave head imaging system for intracranial haemorrhage detection," *PloS One*, Vol. 11, e0152351, 2016.
29. Zubal Phantom Data, [Online]. Available: http://noodle.med.yale.edu/phantom/getdata.htm.
30. Cole, K. S. and R. H. Cole, "Dispersion and absorption in dielectrics I. Alternating current characteristics," *The Journal of Chemical Physics*, Vol. 9, 341–351, 1941.
31. Gabriel, C., S. Gabriel, and E. Corthout, "The dielectric properties of biological tissues: I. Literature survey," *Physics in Medicine and Biology*, Vol. 41, 2231, 1996.
32. Gabriel, S., R. W. Lau, and C. Gabriel, "The dielectric properties of biological tissues: II. Measurements in the frequency range 10 Hz to 20 GHz," *Physics in Medicine and Biology*, Vol. 41, 2251, 1996.
33. Gabriel, S., R. Lau, and C. Gabriel, "The dielectric properties of biological tissues: III. Parametric models for the dielectric spectrum of tissues," *Physics in Medicine and Biology*, Vol. 41, 2271, 1996.
34. Gabriel, C., "Compilation of the dielectric properties of body tissues at RF and microwave frequencies," DTIC Document, 1996.
35. Gabriel, C., A. Peyman, and E. H. Grant, "Electrical conductivity of tissue at frequencies below 1 MHz," *Physics in Medicine and Biology*, Vol. 54, 4863-78, Aug. 21, 2009.
36. Andreuccetti, D., R. Fossi, and C. Petrucci, "Dielectric properties of body tissues," *Applied Physics — Italian National Research Council*, Florence, Italy, 2002, Online: http://niremf.ifac.cnr.it/tissprop/htmlclie/htmlclie.php.
37. Ireland, D. and A. Abbosh, "Modeling human head at microwave frequencies using optimized Debye models and FDTD method," *IEEE Transactions on Antennas and Propagation*, Vol. 61, 2352–2355, 2013.
38. Mustafa, S., A. M. Abbosh, and P. T. Nguyen, "Modeling human head tissues using fourth-order Debye model in convolution-based three-dimensional finite-difference time-domain," *IEEE Transactions on Antennas and Propagation*, Vol. 62, 1354–1361, 2014.
39. Pastorino, M., *Microwave Imaging*, Vol. 208, John Wiley & Sons, 2010.
40. Klemm, M., J. A. Leendertz, D. Gibbins, I. J. Craddock, A. Preece, and R. Benjamin, "Microwave radar-based differential breast cancer imaging: Imaging in homogeneous breast phantoms and low contrast scenarios," *IEEE Transactions on Antennas and Propagation*, Vol. 58, 2337–2344, 2010.
41. Joachimowicz, N., C. Pichot, and J.-P. Hugonin, "Inverse scattering: An iterative numerical method for electromagnetic imaging," *IEEE Transactions on Antennas and Propagation*, Vol. 39, 1742–1753, 1991.

42. Davidson, D. B., "Computational Electromagnetics for RF & microwave engineering," *IEEE Aerospace and Electronic Systems Magazine*, Vol. 20, 27, 2005.
43. Semenov, S., J. Kellam, P. Althausen, T. Williams, A. Abubakar, A. Bulyshev, et al., "Microwave tomography for functional imaging of extremity soft tissues: Feasibility assessment," *Physics in Medicine and Biology*, Vol. 52, 5705, 2007.
44. Ireland, D., K. Bialkowski, and A. Abbosh, "Microwave imaging for brain stroke detection using born iterative method," *IET Microwaves, Antennas & Propagation*, Vol. 7, 909–915, 2013.
45. Zakaria, A., I. Jeffrey, and J. LoVetri, "Full-vectorial parallel finite-element contrast source inversion method," *Progress In Electromagnetics Research*, Vol. 142, 463–483, 2013.
46. Morega, M. and A. M. Morega, "Computed SAR in human head for the assessment of exposure from different phone device antennas," *Environment Engineering and Management Journal*, Vol. 10, 527–533, 2011.
47. Wessapan, T., S. Srisawatdhisukul, and P. Rattanadecho, "Specific absorption rate and temperature distributions in human head subjected to mobile phone radiation at different frequencies," *International Journal of Heat and Mass Transfer*, Vol. 55, 347–359, 2012.
48. Yasin Citkaya, A. and S. Selim Seker, "FEM modeling of SAR distribution and temperature increase in human brain from RF exposure," *International Journal of Communication Systems*, Vol. 25, 1450–1464, 2012.
49. Abdulrazzaq, S. A. and A. P. D. J. S. Aziz, "SAR simulation in human head exposed to RF signals and safety precautions," *Int. J. Comput. Sci. Eng. Technol*, Vol. 3, 334–340, 2013.
50. Sallomi, A., "A theoretical approach for SAR calculation in human head exposed to RF signals," *Journal of Engineering an d Development*, Vol. 16, 2012.
51. "IEEE standard for safety levels with respect to human exposure to radio frequency electromagnetic fields, 3 kHz to 300 GHz," *IEEE Std C95.1-2005 (Revision of IEEE Std C95.1-1991)*, 1–238, 2006.
52. "Guidelines for limiting exposure to time-varying electric, magnetic, and electromagnetic fields (up to 300 GHz)," *Health Phys.*, Vol. 74, 494–522, 1998.